# MODELING OF COMPLEX FRACTURE PROCESSES IN QUASI-BRITTLE MATERIALS

**Rena C. Yu and Gonzalo Ruiz**

**Universidad de Castilla-La Mancha**
**ETS de Ingenieros de Caminos, 13071 Ciudad Real.**

**Resumen.**Esta comunicación presenta una modelización de procesos complejos de fractura en materiales cuasi-frágiles en régimen estático. Usamos una metodología que consiste en combinar modelos cohesivos con un algoritmo de fragmentación. La formación de superficie de fractura se simula insertando elementos cohesivos entre los elementos que modelizan el slido cuando se cumple la condición de apertura. Este proceso genera un alto grado de no linealidad, material y geométrica, que es difícil de tratar con métodos de resolución directos. Aquí salvamos dicha dificultad recurriendo a un método explícito de relajación dinámica para obtener la solución en régimen estático. Validamos el código simulando ensayos de flexión en tres puntos en vigas de hormigón de varios tamaños. El modelo reproduce con fidelidad las tendencias de los ensayos, en particular el efecto de escala experimental.

**Abstract.** This paper analyzes static multi-cracking fracture processes in plain concrete.We use a methodology consisting of combining cohesive theories of fracture together with a novel fragmentation algorithm to model the fracture process. The formation of cohesive surface within the solid is simulated by inserting cohesive elements at the interface between existing elements when the opening condition is attained. Such process generates high geometrical and material nonlinearities which are difficult to handle by direct solvers. As an alternative, we choose an explicit dynamic relaxation method to get the static solution. The code is validated against experimental data from concrete beams loaded at three points. The model closely follows the experimental trends. Particularly, it accurately predicts the load peak for several sizes, thus reproducing the experimentally observed size effect.

## 1 INTRODUCTION

The dynamic behavior of brittle materials, including glass, ceramics, rocks and concrete, which often involves complex fracture and fragmentation processes, has been thoroughly studied by Ortiz and co-workers [1, 2, 3, 4]. The feasibility of cohesive theories of fracture applied to the dynamic regime has also been demonstrated by [5, 6]. However, the modeling of crack propagation within static regime has been hindered by the difficulties to find efficient and stable numerical algorithms which are able to deal with high geometric and material nonlinearities. Implicit solvers such as Newton-Raphson or quasi-Newton schemes may not provide either stable or converged solutions. Explicit dynamic relaxation method, as an alternative, avoids the use of direct solvers and makes it specially attractive in computational mechanics, since all quantities are treated as vectors and the large storage requirements associated with large matrices are avoided.

The idea behind dynamic relaxation is based on viewing the solution of a static problem as the steady-state solution of a damped wave equation. Since the transient part of the solution is not of interest, the corresponding dynamic problem can be chosen in such a way that the rate of convergence to the steady-state is maximized. This is often realized by adding fictitious inertia and damping terms to the real static problem.

First applications of dynamic relaxation method to solve linear structural problems were developed by Otter [7] and Day [8], along with Welsh [9] and Wood [10] in the 1960s. More papers [11, 12] in the 1970s showed the efficiency and capability to solve complex engineering problems. In early 1980s, Underwood [13] gave an thorough review on the methodology, selection of integration parameters (fictitious mass and damping matrices), as well as an adaptive algorithm to evaluate those parameters for high nonlinear problems. Following the ideas given by Underwood, Sauve and Metzger [14] as well as many others showed the reliability of dynamic relaxation method in solving problems involving geometric and material nonlinearities, incompressibility conditions and creep.

We implement the ideas by Underwood for fictitious mass and critical damping coefficients. A combined convergence criteria of kinetic energy and out-of-balance forces is used. Next, a brief introduction of the cohesive model is given; the formulation of the explicit dynamic relax-

ation method is presented afterwards and the simulations results as well as the comparisons with the experiments are discussed at the end.

## 2 THE COHESIVE MODEL

For completeness, in this section we summarize the main features of the cohesive law used in the calculations. An extensive account of the theory and its finite-element implementation may be found elsewhere [1, 2]. A simple class of mixed-mode cohesive laws accounting for tension-shear coupling [1, 2, 15], is obtained by the introduction of an effective opening displacement $\delta$, which assigns different weights to the normal $\delta_n$ and sliding $\delta_S$ opening displacements.

$$\delta = \sqrt{\beta^2 \delta_S^2 + \delta_n^2} \tag{1}$$

Assuming that the cohesive free-energy density depend on the opening displacements only through the effective opening displacement $\delta$, a reduced cohesive law, which relates $\delta$ to an effective cohesive traction

$$t = \sqrt{\beta^{-2}|t_s|^2 + t_n^2} \tag{2}$$

where $t_s$ and $t_n$ being the shear and the normal tractions, respectively, can be obtained [1, 2]. It is observed that the weighting coefficient $\beta$ defines the ratio between the shear and the normal critical tractions (and thus it also roughly defines the ratio of $K_{IIc}$ to $K_{Ic}$). Assuming the existence of a loading envelope defining a relation between $t$ and $\delta$ under the conditions of monotonic loading, and that unloading is irreversible, a simple and convenient type of irreversible cohesive law is furnished by the linearly decreasing envelope described in Eqn (3), where $\sigma_c$ is the tensile strength, $\delta_c$ the critical opening displacement and $G_c = 1/2\sigma_c\delta_c$ is the specific fracture energy. Similarly, a bilinear cohesive law according to the Model Code [16] for concrete can be defined through the softening law characterized in Eqn. (4).

$$t = \begin{cases} \sigma_c(1 - \delta/\delta_c) & 0 \le \delta \le \delta_c \\ 0 & \delta \ge \delta_c \end{cases} \tag{3}$$

$$t = \begin{cases} \sigma_c(1 - 0.85\delta/\delta_c) & 0 \le \delta \le \delta_A \\ 0.15\sigma_c(\delta_c - \delta)/(\delta_c - \delta_A) & \delta_A \le \delta \le \delta_c \\ 0 & \delta \ge \delta_c \end{cases} \tag{4}$$

where $\delta_A$ and $\delta_c$ are determined through the following equations

$$\begin{aligned} \delta_A &= (2 - 0.15\beta_F)G_c/\delta_c \\ \delta_c &= \beta_F G_c/\delta_c \end{aligned}$$

$\beta_F$ is related to the maximum aggregate size $d_{max}$, for the case of $d_{max} = 5$ mm, $\beta_F$ can be taken roughly to be 8.4 [17], which is used in the simulations later on.

Cohesive theories introduce a well-defined length scale into the material description and, in consequence, are sensitive to the size of the specimen (see, for example, [18]). The characteristic length of the material may be expressed as

$$l_{ch} = \frac{EG_c}{f_{ts}^2} \tag{5}$$

where $E$ is the elastic modulus and $f_{ts}$ the static tensile strength.

In calculations, only decohesion along element boundaries is allowed to occur. Initially, all element boundaries are perfectly coherent and the elements conform in the usual sense of the displacement finite element method. When the critical cohesive traction is attained at the interface between two volume elements, a cohesive element is inserted at that location using a fast algorithm [19]. The cohesive element subsequently governs the opening of the cohesive surface.

## 3 FORMULATION OF THE EXPLICIT DYNAMIC RELAXATION METHOD

As we mentioned before, in calculations, the fracture surface is confined to inter-element boundaries and, consequently, the structural cracks predicted by the analysis are necessarily rough. Even though this numerical roughness in concrete can be made to correspond to the physical roughness by the simple device of choosing the element size to resolve the cohesive zone size [4], the nonlinearity of the solution thus induced plus the material nonlinearity is difficult to handle in static regime for traditional solvers. We choose explicit dynamic relaxation method as an alternative to tackle this situation, the formulation of this methodology is given below.

Consider the semi-discrete governing equation for a static problem at a certain loading step $n$

$$F_n^{int}(x_n) = F_n^{ext} \tag{6}$$

where $x_n$ is the solution array (displacements), $F_n^{int}$ and $F_n^{ext}$ are internal and external force vectors. Following the ideas of dynamic relaxation, Eqn. (6) is transformed to a dynamic system by adding both inertia and damping terms.

$$M\ddot{x}_n + D\dot{x}_n = R_n \tag{7}$$

where $M$ and $D$ are the fictitious mass and damping matrices, $\ddot{x}_n$ and $\dot{x}_n$ are acceleration and velocity vectors respectively, $R_n = F_n^{ext} - F_n^{int}(x_n)$ is the out-of-balance residual forces at load step $n$.

The solution of Eqn. (7) is obtained by the explicit time integration method using the central difference integration scheme in two steps. First the displacements and predictor velocities are obtained

$$x_n^{t+1} = x_n^t + \triangle t \dot{x}_n^t + \frac{1}{2}\triangle t^2 \ddot{x}_n^t \tag{8}$$

$$\dot{x}_n^{t+\triangle t/2} = \dot{x}_n^t + \frac{1}{2}\triangle t\ddot{x}_n^t \quad (9)$$

Second we update the internal force vector and obtain the accelerations and corrected velocities.

$$\ddot{x}_n^{t+1} = (M + \frac{1}{2}\triangle tD)^{-1} [R(x_n^{t+1}) - D\dot{x}_n^{t+\triangle t/2}] \quad (10)$$

$$\dot{x}_n^{t+1} = \dot{x}_n^{t+\triangle t/2} + \frac{1}{2}\triangle t\ddot{x}_n^{t+1} \quad (11)$$

In order to preserve the explicit form of the time-stepping integrator, both fictitious mass $M$ and damping $D$ matrices are set to be diagonal. At the same time, the damping matrix is chosen to be proportional to the mass matrix through a damping coefficient $\xi$, which is going to be determined in the calculations.

### 3.1 Evaluation of the fictitious mass matrix

As aforementioned, the dynamic relaxation parameters can be selected to produce fastest and most stable convergence to the static solution of the real physical system. These parameters includes the mass matrix $M$, the damping coefficient $\xi$ and time step $\triangle t$. Owing to the explicit formulation, the time step must satisfy the stability condition, $\triangle t \leq 2/\omega_{max}$, where $\omega_{max}$ is the highest undamped frequency of the discretized system, which can be estimated as $\omega^e_{max} = 2c_e/h_e$. where $c_e$ is the dilatational wave speed of the material ($c_e^2 = (\lambda + 2G)/\rho_e$), $h_e$ represents the size of the element. This condition provides a relation between the maximum admissible fictitious time step $\triangle t_{cr} = 2/\omega_{max}$ and the fictitious mass matrix.

$$\rho_e \geq (\lambda + 2G)\left(\frac{\triangle t_{cr}}{h_e}\right)^2 \quad (12)$$

In calculations, the fictitious time step $\triangle t_{cr}$ is set to be 1, the mass of each element is computed accordingly.

### 3.2 Estimation of the fictitious damping matrix

In Underwood [20], the convergence rate of dynamic relaxation is given in terms of the spectral radius of the iterative error equations

$$R \approx \mid 1 - 2\frac{\omega_{min}}{\omega_{max}} \mid \quad (13)$$

where $\omega_{min}$ and $\omega_{max}$ are the lowest and highest frequencies of the discretized equations of motion. By maximizing the ratio $\omega_{min}/\omega_{max}$ , and therefore minimizing $R$, a faster convergence rate can be obtained. The highest frequency $\omega_{max}$ is mesh and material dependent, whereas $\omega_{min}$ is based on the lowest participating mode of the structure corresponding to the load distribution. For models where the mode of loading corresponding to a very low structural frequency and the mesh discretization is such that the local element frequencies are high, a slower convergence rate can be expected [14]. By adjusting the mass matrix and choosing a suitable time step, this effect can be minimized. In the present work, the scheme to estimate the critical damping coefficient ($\xi = 2\omega_{min}$) suggested by Underwood is implemented. The current value of $\omega_{min}$ is estimated at each iteration $t$ using Rayleigh quotient

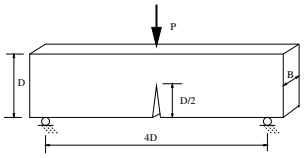


Figure 1: A concrete beam subjected to three point bending.

$$\omega^t_{min} = \sqrt{\frac{(\omega^t)^T K^t \omega^t}{(\omega^t)^T M^k \omega^t}} \quad (14)$$

where $\omega^t$ stands for the eigenvector associated to $\omega^t_{min}$ and $M$ is the mass matrix at $t^{th}$ iteration. For nonlinear problems, $K$ represents a diagonal estimate of the tangent stiffness matrix at the $t^{th}$ iteration and is given by

$$K^t_{ii} = \frac{F_i^{int}(x_n^t) - F_i^{int}(x_n^{t-1})}{x_n^t - x_n^{t-1}} \quad (15)$$

### 3.3 Convergence criteria

In dealing with convergence problems, it is highly desirable to choose a criteria that will neither lead to unproductive cycles nor inaccurate results. In this work, taking into consideration the specific problem we are trying to solve, a combined convergence criteria is implemented. One is the ratio between the residual forces and the estimated maximum external forces, the measure that says how far is the solution from equilibrium, the other is the global kinetic energy, which measures whether the loading is static or not. This combined criteria is characterized by the following inequalities

$$\frac{\parallel R \parallel_2}{\parallel F^{ext} \parallel_2} < f_{tol} \quad (16)$$

$$\sum M(\dot{x}^t)^2 < ke_{tol} \quad (17)$$

where $\parallel . \parallel_2$ denotes the Euclidean norm. The tolerances $f_{tol}$ and $ke_{tol}$ are taken as 0.001 and $10^{-8}\ N \cdot mm$ respectively. For the problems we have considered, these tolerances provide a good balance of accuracy and efficiency.

## 4 NUMERICAL ANALYSIS

We apply the dynamic relaxation method to solve the static propagation of a crack through a notched concrete beam subjected to three point bending, see Figure (1).

Table 1: Concrete mechanical properties

| $f_t$ (MPa) | E (GPa) | $G_c$ (N/m) | $l_{ch}$ (mm) |
|---|---|---|---|
| 3.8 | 30.5 | 62.5 | 130 |

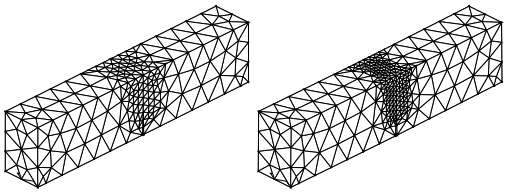

(a) (b)

Figure 2: The meshes used in the simulations for specimen A1 ($D = 75$ mm); element size at middle surface (a) 6 mm; (b)3 mm.

Two specimens, one with depth $D = 75$ mm (specimen A1), the other one with depth $D = 150$ mm (specimen A2), both with the same thickness $B = 50$ mm are modeled. Both specimens are discretized into ten-node quadratic tetrahedral elements and have element size of 6 mm near the middle surface. The material parameters are given in Table 1.

### 4.1 Mesh dependency

In previous studies, Camacho and Ortiz [1] have noted that the accurate description of fracture processes by means of cohesive elements requires the resolution of the characteristic cohesive length of the material. Ruiz et al. [4] pointed out that in concrete, the element size can be made to be comparable to the maximum aggregate size, which is 5 mm in this case. Here, we compare the load curve results from a coarse mesh 1 (element size 6 mm, 3556 nodes, 2103 tetrahedron) and a finer mesh 2 (element size 3 mm, 6283 nodes, 3950 tetrahedron) in Figure (3). The loading path from mesh 1 and 2 as well as the peak load are in good agreement, while the computations for mesh 1 would be much more efficient, so the following simulations are based on this mesh for specimen A1 and the mesh of similar size for specimen A2.

### 4.2 Peak load comparison

According to the work of Bažant and Planas [18], the peak load is directly related to the initial slope of the cohesive law of the material.The fracture parameters are chosen to meet the initial slope (the ratio of $\sigma_c/\delta_c$ in Eqn (3)) suggested by Ruiz [17] and the static tensile strength is according to the experiments, i.e., $\sigma_c = 3.8MPa$, $\delta_c = 14.5\mu m$. This gives a fracture energy

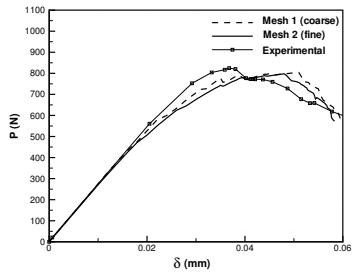


Figure 3: The load curve comparison for mesh 1 and 2 and compared with experimental results.

(27.55 N/m) smaller than in the experiments (62.5 N/m), which leads to the quick drop of the loading forces compared to its experimental counterpart. This can be corrected by the bilinear cohesive law in Eqn (4) which reflects both the initial slope and the specific fracture energy correctly. The load versus displacement curve for specimen A1 and A2, compared with the experimental results are shown in Figure (4). An agreement of $0.4\%$ for specimen A1 and $3.0\%$ for specimen A2 under both cohesive laws is achieved. For the case of bilinear cohesive law, the numerical curve also follows the experimental results closely after the peak load, when the specimen is weakened by the fracture process around the load plane.

Since specimen A1 and A2 are scaled in size, we have set the load and displacement curve for Figure (4)a and Figure (4)b proportional, the experimentally observed size effect - the maximum load withstood by the beams increases at a slower rate than the beam dimensions - is also well represented in the simulations.

### 4.3 Fracture patterns

Three snapshots of the fracture patterns on mid-plane for specimen A1 is shown in Figure (5), where the displacements have been magnified 100 times to aid visualization. Figure (5)a is the point of peak load, Figure (5)c is the moment where the beam is almost completely crushed, while Figure (5)b is a point in between which shows how the fracture zone has developed. Also shown in the figures are the level contours of damage, defined as the fraction of expended fracture energy to total fracture energy per unit surface, or critical energy release rate. Thus, a damage density of zero denotes an uncracked surface, whereas a damage density of one is indicative of a fully cracked or free surface. The transition zone wherein the damage variable takes intermediate values may be regarded as the cohesive zone, and the crack front may conventionally be identified with the level contour of 1/2. It can be noticed that in the peak load, Figure (5)a, the fracture zone has developed to some degree, only that the crack surfaces are not fully open yet; later

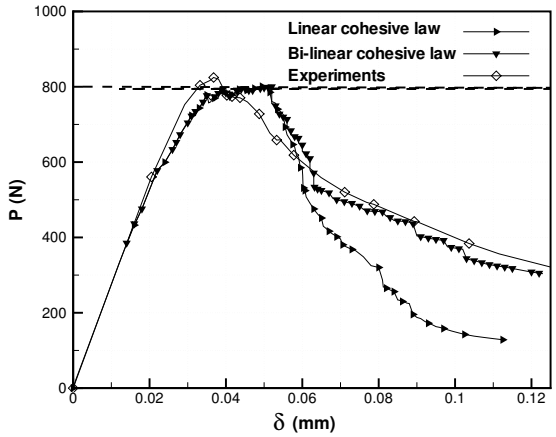


(a)

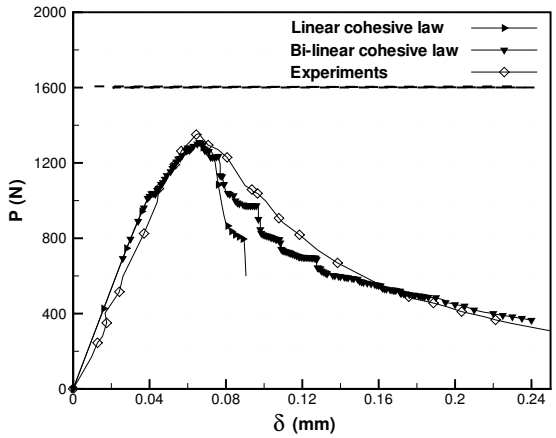


(b)

Figure 4: The $P - \delta$ curve comparison for specimen A1 ($D = 75$ mm) and A2 ($D = 150$ mm) under the linear cohesive law (Eqn (3)) and the bi-linear cohesive law (Eqn. (4)), compared with the experimental results.

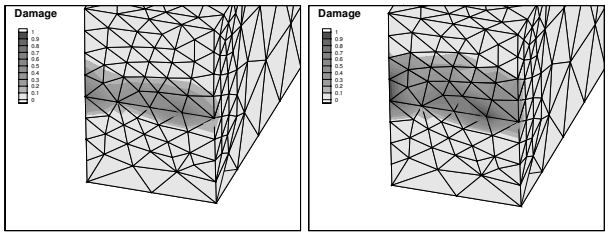


(a) (b)

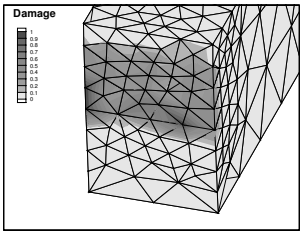


(c)

Figure 5: Snapshots of the fracture patterns developed at loading displacement (a) 0.05 mm (near peak load); (B) 0.07 mm; and (c) 0.11 mm respectively.

on in Figure (5)b, the same zone is more developed while new surfaces are open and the crack front propagates in a nonuniform way, which can only be observed in a full three-dimensional modeling. It is interesting to note that the crack front is convex in the direction of propagation, a feature which is characteristic of mode-I crack growth, the exterior of the crack front ostensibly lags behind the interior points. In Figure (5)c, the crack continues to grow till the specimen is almost completely crushed and loses its strength.

## 5 SUMMARY AND CONCLUSIONS

We have put together the explicit dynamic relaxation method in conjunction with the cohesive theory to solve the static multi-cracking fracture process in a three-point-bend concrete beam. In calculations, the fracture surface is confined to inter-element boundary elements and, consequently, the structural cracks predicted by the analysis are necessarily rough. Even though, this numerical roughness in concrete can be made to correspond to the physical roughness by choosing the element size comparable to the aggregate size, the thus-induced geometrical nonlinearity and the material nonlinearity inherent to concrete are hard to handle for traditional static solvers. Explicit dynamic relaxation method, as an alternative, avoids the use of direct solvers as well as the large storage requirements associated with large matrices, makes it specially attractive in computational mechanics [14]. We

follow the ideas of Underwood [20] for fictitious mass and damping matrices and implemented the explicit dynamic relaxation method. A combined convergence criterion of relative residual forces and global kinetic energy is chosen to provide a good balance of accuracy and efficiency. Two sizes of concrete beams were modeled to validate against the experimental results of Ruiz [17]. The preliminary results show the model captures the peak load accurately. Explicit dynamic relaxation method seems promising as an viable alternative in providing an efficient and accurate solutions to static problems when high nonlinearities are involved.

## 6 ACKNOWLEDGMENTS

Rena C. Yu and Gonzalo Ruiz thank the *Ministerio de Educación, Cultura y Deporte*, Spain, for the scholarship SB2000-0191, which makes possible their joint work at the *ETSI de Caminos, C., y P., Universidad de Castilla-La Mancha* (UCLM). Gonzalo Ruiz acknowledges financial support from the *Ministerio de Ciencia y Tecnología*, Spain, under grant MAT2000-0705, and the UCLM, Spain, under grant 011,1075.

## REFERENCES

[1] G. T. Camacho and M. Ortiz. Computational modelling of impact damage in brittle materials. *International Journal of Solids and Structures*, 33 (20-22):2899–2938, 1996.

[2] M. Ortiz and A. Pandolfi. Finite-deformation irreversible cohesive elements for three-dimensional crack-propagation analysis. *International Journal for Numerical Methods in Engineering*, 44:1267–1282, 1999.

[3] G. Ruiz, M. Ortiz, and A. Pandolfi. Three-dimensional finite-element simulation of the dynamic Brazilian tests on concrete cylinders. *International Journal for Numerical Methods in Engineering*, 48:963–994, 2000.

[4] G. Ruiz, A. Pandolfi, and M. Ortiz. Three-dimensional cohesive modeling of dynamic mixed-mode fracture. *International Journal for Numerical Methods in Engineering*, 52:97–120, 2001.

[5] A. Pandolfi, P. Krysl, and M. Ortiz. Finite element simulation of ring expansion and fragmentation. *International Journal of Fracture*, 95:279–297, 1999.

[6] C. Yu, A. Pandolfi, D. Coker, M. Ortiz, and A.J. Rosakis. Three-dimensional Modeling of Intersonic Shear-CRack Growth in Asymmetrically-Loaded Unidirectional Composite Plates. *International Journal of Solids and Structures*, 39(25):6135–6157, 2002.

[7] J.R.H. Otter. Computations for prestressed concrete reactor pressure vessels using dynamic relaxation. *Nucl. Struct. Engng.*, 1:61–75, 1965.

[8] A.S. Day. An introduction to dynamic relaxation. *The Engineer*, 219:218–221, 1965.

[9] A.K. Welsh. Discussion on dynamic relaxation. *Proc. Inst. Civ. Engrs.*, 37:723–750, 1967.

[10] W.L. Wood. Comparison of dynamic relaxation with three other iterative methods. *Engineer*, 224:683–687, 1967.

[11] A.C. Cassell. Shell of revolution under arbitrary loading and the use of ficticious densities in dynamic relaxation. *Proc. Inst. Civ. Engrs.*, 45:65–78, 1970.

[12] A.C. Cassell and R.E. Hobbs. Numerical stability of dynamic relaxation structural analysis. *International Journal for Numerical Methods in Engineering*, 10:1407–1410, 1976.

[13] P.G. Underwood and K. C. Park. A variable-step central difference method for structural dyanmics analysis - part 2. implementation and performance evaluation. *Transactions of the ASME*, 23:259–279, 1980.

[14] R. G. Sauve and D.R. Metzger. Advances in dynamic relaxation techniques for nonlinear finite element analysis. *Transactions of the ASME*, 117:170–176, 1995.

[15] A. De Andrés, J. L. Pérez, and M. Ortiz. Elastoplastic finite-element analysis of three-dimensional fatigue crack growth in aluminum shafts subjected to axial loading. *International Journal of Solids and Structures*, 36(15):2231–2258, 1999.

[16] Subcommitee CEN/TC 250/SC2. Eurocode 2: Project of concrete structures. *AENOR*,Madrid,Spain,1993.

[17] G. Ruiz. Influencia del Tamaño y de la Adherencia en la Armadura Mínima de Vigas en Flexión. *Grupo Español del Hormigón*, Madrid, Spain, 1998.

[18] Z. P. Bažant and J. Planas. *Fracture and Size Effect in Concrete and Other Quasibrittle Materials*. CRC Press, Boca Raton, Florida, 1998.

[19] A. Pandolfi and M. Ortiz. An Efficient Adaptive Procedure for Three-Dimensional Fragmentation Simulations. *Engineering with Computers*, 18(2):148–159, 2002.

[20] P.G. Underwood. Dyanmic relaxation. *Computational Methods for Transient Analysis*, 1:145–265, 1983.